



Article

The Effects of Lockdown, Urban Meteorology, Pollutants, and Anomalous Diffusion on the SARS-CoV-2 Pandemic in Santiago de Chile

Patrício Pacheco ^{1,*}, Eduardo Mera ¹ and Gustavo Navarro ²

¹ Departamento de Física, Facultad de Ciencias Naturales, Matemáticas y Medio Ambiente, Universidad Tecnológica Metropolitana, Las Palmeras 3360, Ñuñoa 7750000, Chile; emera@utem.cl

² Departamento de Ciencias Exactas, Facultad de Ingeniería, Arquitectura y Diseño, Universidad de San Sebastián, Bellavista 7, Recoleta, Santiago 8420000, Chile; gustavo.navarro@uss.cl

* Correspondence: patrício.pacheco@utem.cl

Abstract: A study was carried out in Santiago de Chile, located in a geographic basin, on the sustainability and diffusion of the recent SARS-CoV-2 pandemic. Hourly measurements were used (carried out for 3.25 years in seven communes of the city) to quantify the accumulated sick (AS) population, urban meteorology variables (MVs) (temperature (T), relative humidity (RH), and magnitude of wind speed (WS)), and air pollution (P) (PM_{10} , $PM_{2.5}$, O_3). Time series (TS) were constructed for each commune, which related AS to MVs, called AS/VM, and to P, noted AS/P. Chaos theory was applied to each TS, requiring the following variables: the Lyapunov exponent ($\lambda > 0$), the correlation dimension ($D_C < 5$), Kolmogorov entropy ($S_K > 0$), the Hurst exponent (H , such that $0 < H < 1$), Lempel-Ziv complexity ($LZ > 0$), and information loss ($\langle \Delta I \rangle < 0$). Every TS complied with chaos theory. For each commune, C_K was calculated as a quotient between the sum of AS/T, AS/WS, and AS/RH entropies and the sum of AS/ PM_{10} , AS/ $PM_{2.5}$, and AS/ O_3 entropies. The results show that the entropy for the AS/P ratio is lower than that of the AS/VM ratio in three of the seven communes, since between 2020 and early 2022, the population was confined, reducing pollution. The TS of the AS/P ratio is more persistent and complex. The predictability times of the ratios are comparable in four of the seven communes. The TS of the AS/MV ratios shows greater information loss and chaos. According to the calculated C_K values, it is possible to relate it to anomalous diffusion (sub/super-diffusion) and the context that favored the expansion of the pandemic: urban densification, pollution, urban meteorology, population density, etc. Using Fréchet heavy-tailed probability, the compatibility of the results with C_K is verified.

Keywords: accumulated sick; pollutant; urban meteorology; entropy; loss of information; diffusion



Citation: Pacheco, P.; Mera, E.; Navarro, G. The Effects of Lockdown, Urban Meteorology, Pollutants, and Anomalous Diffusion on the SARS-CoV-2 Pandemic in Santiago de Chile. *Atmosphere* **2024**, *15*, 414.

<https://doi.org/10.3390/atmos15040414>

Academic Editor: Andreas Matzarakis

Received: 31 January 2024

Revised: 11 March 2024

Accepted: 19 March 2024

Published: 26 March 2024



Copyright: © 2024 by the authors. Licensee MDPI, Basel, Switzerland. This article is an open access article distributed under the terms and conditions of the Creative Commons Attribution (CC BY) license (<https://creativecommons.org/licenses/by/4.0/>).

1. Introduction

A geographical basin corresponds to an area surrounded by mountains that make it difficult to ventilate and expose it, in times of climate change, to extended periods of drought and an increase in temperature [1]. Urban densification also contributes to this, especially with high-rise buildings [1,2]. These same conditions can contribute to the persistence of diseases with varied characteristics that affect the population [3,4]. Santiago de Chile is a geographical basin where the most complex period of the SARS-CoV-2 pandemic (without differentiating variants) occurred from 31 March 2020 to March 2022, because of the number of accumulated patients and the waves of contagion [3,4]. While time series do not validate lockdowns, they can suggest that a lockdown decision was correct. In Santiago de Chile, the time series of accumulated sick people versus temperature displayed a greater LZ complexity (which describes the regularity of a sequence, where the more repeated sub-sequences that appear as you scan from left to right, the lower the value of LZ) with respect to the other meteorological variables, which is consistent with the

presence of thermal islands [4]. It also showed, in most cases, a greater persistence, wherein the past influenced the future. The average value of the Hurst coefficient (persistence in the future) and the Lempel-Ziv complexity for the time series of accumulated sick people versus pollutants was larger than that of the time series of accumulated sick people versus urban meteorology. From the perspective of square meters built, it was shown that there was a relationship between communes with large built areas and those with the highest number of accumulated patients. Intensive urbanization and densification were predicted to contribute to the urban stagnation of the pandemic [4]. The current urban plan has become critical for the quality of life of people in relation to the environment.

In [3], a study carried out for a period of 2.5 months (30 March–15 June 2022) showed that micrometeorology (a part of meteorology that deals with observations and processes on the smallest scales of time and space, of approximately less than 1 km and short periods) and air pollution variables were part of the factors that allowed for the continuous accumulated growth of infected patients, favoring the pandemic's spread, making the curve of accumulated sick people chaotic, and increasing its complexity. Furthermore, environmental pollution was predicted to make diseases like the COVID-19 coronavirus worse. Expanding the data recording period to 25 months (30 March 2020 to 18 April 2022), the investigation in [4] found that the entropies of the time series of accumulated sick people versus pollutants were still greater than the entropies of the series of accumulated sick people versus urban meteorology. The commune of Puente Alto, with an intensive housing construction process, had the largest communal population in Chile and the largest number of accumulated sick people in the metropolitan region; it also presented the largest entropic gap in favor of pollutants. This contributed to its atmosphere being very polluted and conditions that favored the spread of the virus [5]. As of mid-2022, the measures implemented to control the spread of the pandemic were relaxed, although the vaccination process was maintained, increasing the number of doses per person. In this research, we aimed to comparatively study the pandemic timeline by examining the results of an extended period of data collection from 31 March 2020 to 9 January 2023, which includes the confinement of the population and a decrease in activities (transport, educational centers, only essential industries, etc.). This study investigates the following questions: By reducing high values, does confinement moderate variations in the time series of accumulated sick people versus pollutants and/or of accumulated sick people versus urban meteorology? If pollution decreases, after almost 2 years of confinement, is it still relevant in the sustainability of the time series of accumulated patients or does urban meteorology (represented in this study by T, RH, and WS) become more important?

Science in the 21st century has been moving towards systems approaches, interdisciplinary perspectives, and the concepts of complexity theories. The central characteristic of complex systems is the low predictability of their macroscopic properties and their temporal evolution. Probability theory, statistics, and the emerging areas of data science and deep learning are expected to play great roles in the construction of ideas. Regarding complex systems, it has been observed on many occasions that the properties of interest follow heavy-tailed probability distributions.

When a phenomenon follows a heavy-tailed distribution, statistics such as the mean and sample variance are not informative since there is no characteristic scale for the occurrence of the phenomenon. In this type of system, extreme events have a relatively high probability of occurring. Many times, extreme events are more interesting to understand and predict than accumulated non-extreme events since their impact is much greater, as seen with climate change, heat waves, pollution interactions, urban meteorology, the outbreak of pandemics, large earthquakes, etc. Within the theory of complex systems, the classic model that is used to describe heavy-tailed phenomena is the power law, but probability distributions such as Fréchet, Cauchy, LogNormal, Pareto, Student's t, and Zipf are also good descriptors.

There are theoretical mechanisms that explain the appearance of the power law, and there is evidence that many phenomena are governed by this type of law. Validating them using empirical data is a task that is far from simple, apart from there being theoretical

reasons indicating that these systems experience, in practice, effects of finite size, imposing at least two domains of description including large scales and small scales.

To answer these questions, measurements made in seven different locations in Santiago de Chile are used. These measurements are time series (each with 24,360 data points (hour) = 24 h/days × (276 days + 365 days + 365 days + 9 days) of temperature, relative humidity, wind speed magnitude, particulate matter (10 and 2.5 μm), and O_3 . From these data and the accumulated sick (AS) of each commune, the ratios $X = \text{AS}/T$, $Y = \text{AS}/\text{WS}$, $Z = \text{AS}/\text{RH}$, $U = \text{AS}/\text{PM}_{2.5}$, $W = \text{AS}/\text{PM}_{10}$, and $V = \text{AS}/\text{O}_3$ are constructed. It is assumed that the new time series generated represents irreversible processes, so the data are analyzed through chaos theory. The chaotic parameters calculated for each series must satisfy $\lambda > 0$, $D_C < 5$, $S_K > 0$, $0.5 < H < 1$, and $LZ > 0$. The analysis of these values and their relationships provide criteria that allow for determining the effect of confinement and other measurements at the microscale where the measurements were made (2–10 m).

2. Materials and Methods

2.1. Area of Study

The city of Santiago is located between the coordinates $33^{\circ}26'16''$ S and $70^{\circ}39'01''$ W and at an average altitude of 567 masl (meters above sea level). It has an area of 837.89 km². The city is located mainly on a plain known as the Santiago basin. This basin is part of the Intermediate Depression and is bounded by the Chacabuco mountain range to the north, the Andes Mountains to the east, the Paine Narrows to the south, and the Coastal Mountain Range to the west. The basin is approximately 80 km long in a north–south direction and 35 km from east to west. The city of Santiago contains 6 provinces subdivided into 52 communes with a projected population of 8,367,790 inhabitants in 2023, equivalent to 42% of the national population, with a density of around 400 inhab/km², as shown in Figure 1.

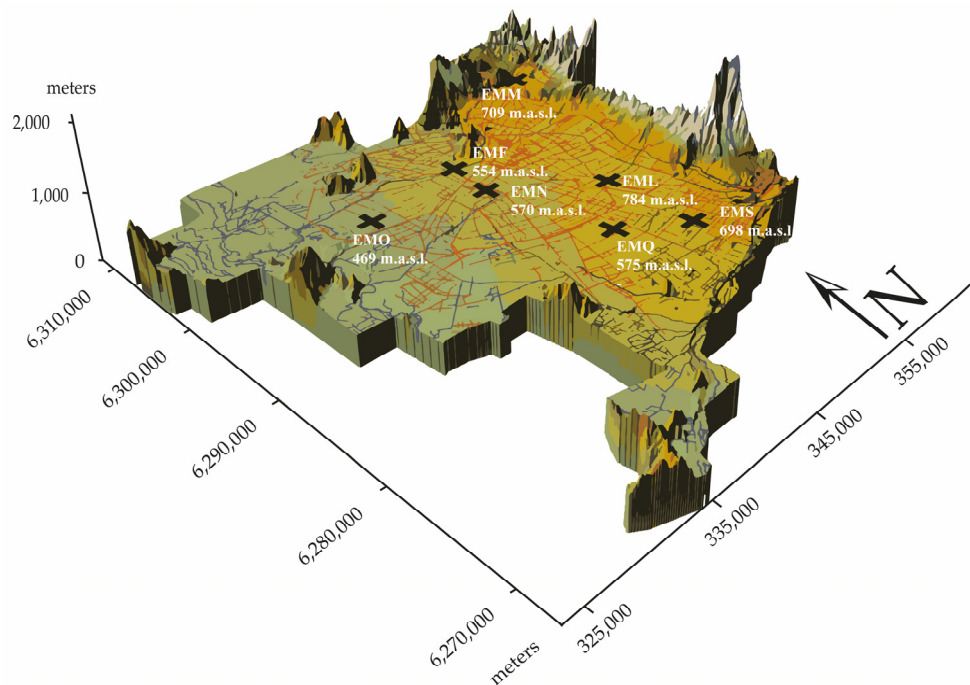


Figure 1. Representation of the studied communes and their geographical position in the Santiago de Chile Basin (EML: La Florida, EMM: Las Condes, EMN: Santiago-Parque O'Higgins, EMO: Pudahuel, EMS: Puente Alto, EMF: Independencia, EMQ: El Bosque).

Table 1 below presents, for each monitoring station, the geographical characteristics of its location, the dominant climatology, the variety of atmospheric pollutants that were measured, the most characteristic wind direction in the year, and the annual averages of the temperature and relative humidity.

Table 1. Information on the station name (with SINCA code in capital letters and meters above sea level (masl)), geography, climate, pollution, dominant wind direction (W), annual average temperature (T), and annual average relative humidity (RH%) for each locality studied (31 March 2020–9 January 2023) [4].

Station Name	Geography	Climate	Pollution	Wind	T (°C) Average Period	RH (%) Average Period
1. La Florida, EML, masl: 784 (m)	Located in the Andes piedmont	Cold, wet winters with little rainfall; hot and dry summers	Presence in descending order PM ₁₀ , CO, PM _{2.5} , NO ₂ , O ₃ , SO ₂	West–east dayEast–west night	15.33	58.85
2. Las Condes, EMM, masl: 709 (m)	Located in the Andes piedmont	Cold, dry winters; hot, dry summers	Presence in descending order PM ₁₀ , CO, PM _{2.5} , NO ₂ , O ₃ , SO ₂	West–east dayEast–west night	13.99	59.44
3. Santiago-Parque O'Higgins, EMN, masl: 570 (m)	Located in the middle of the basin plane	Cold, dry winters; hot, dry summers	Presence in descending order PM ₁₀ , PM _{2.5} , CO, SO ₂ , NO ₂ , O ₃	West–east dayEast–south night	15.26	63.20
4. Pudahuel, EMO, masl: 469 (m)	Located at the bottom of the basin	Cold, dry winters; hot, dry summers	Presence in descending order PM ₁₀ , PM _{2.5} , CO, SO ₂ , NO ₂ , O ₃	South–east dayEast–south night	14.51	63.89
5. Puente Alto, EMS, masl: 698 (m)	Located in the Andes piedmont	Cold, wet winters with moderate rainfall; hot, dry summers	Presence in descending order PM ₁₀ , CO, PM _{2.5} , NO ₂ , O ₃ , SO ₂	West–east dayEast–west night	14.68	58.92
6. Independencia, EMF, masl: 554 (m)	Situated in the intermediate zone of the basin	Cold, dry winters; hot, dry summers	Presence in descending order PM ₁₀ , PM _{2.5} , CO, SO ₂ , NO ₂ , O ₃	North–east day East–south night	15.17	61.18
7. El Bosque EMQ, masl: 575 (m)	Located at the bottom of the basin	Cold, wet winters; hot, dry summers	Presence in descending order PM ₁₀ , PM _{2.5} , NO ₂ , CO, SO ₂ , O ₃	South–east dayEast–south night	13.61	59.09

2.2. The Data

To analyze the coronavirus pandemic [3,4] by applying chaos theory, time series were formed using urban densification (represented by atmospheric pollution), micrometeorology, and information on patients infected and accumulated with SARS-CoV2 (AS) in seven communes in a period of 34.25 months [4].

2.2.1. PM_{2.5} and PM₁₀ Particulate Matter

The harmful effects of pollution by particulate matter [6,7] on human health are known. These range from respiratory tract irritation to cardiovascular diseases. Particulate matter affects all types of surfaces (buildings, public monuments, etc.). It also affects vegetation, decreases visibility, and induces cloud formation [8]. The World Health Organization [9] set the following standards for coarse particles (PM₁₀): 20 µg m⁻³ as an annual average and 50 µg m⁻³ as a 24-hour average. For PM_{2.5}, 10 µg m⁻³ is set as an annual average and 25 µg m⁻³ as a 24-hour average [4].

2.2.2. Tropospheric Ozone (O₃)

Ozone is an oxidant that affects human health. It has been shown [10] that O₃ concentrations damage respiratory function, especially in the summer, causing lung inflammation, respiratory failure, asthma, and other bronchopulmonary diseases. European studies [10] proved that daily deaths increase as exposure to ozone increases. According to [11], extended exposure to ozone has effects including the deterioration of reproductive health. Since 2005, several cohort analyses of long-term ozone exposure and mortality in people with pre-existing conditions have been published. Ozone also impacts vegetation and crops and is currently considered the third most important greenhouse gas (after carbon dioxide and methane). The WHO standard indicates a value of 100 µg m⁻³ for the eight-hour daily average concentration of tropospheric ozone.

As O₃ affects people's respiratory systems, and a pattern of pre-existing diseases was known before the arrival of COVID-19, its choice in this study is natural. The Metropolitan Region has a high densification rate of high-rise buildings, creating a connected urban meteorology that favors urban heat islands and urban canyons [4,12].

2.2.3. Meteorological Variables

The meteorological variables, with which properties of the atmosphere are typically characterized, are used in the form of the following time series in this research: temperature (T), relative humidity (RH), and magnitude of wind speed (WS) [13]. The orography and localized urban climate are also considered to have an impact.

2.2.4. COVID-19 in Santiago de Chile

Waves

The study period covers 34.25 months, from 31 March 2020 to 9 January 2023. This time corresponds to a rapid accumulation of patients in the Metropolitan Region, which overloaded health centers, including three strong waves of contagion that decreased towards the end of 2022, as vaccination became more rigorous, informed, and massive, as shown in Figure 2.

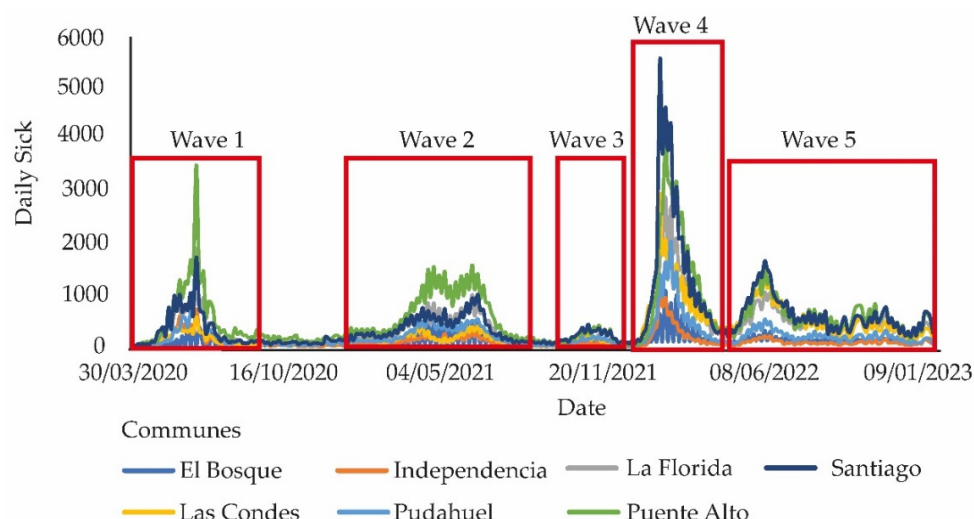


Figure 2. Contagion waves consisting of the maximum number of daily sick patients according to the seven communes [4].

A larger and more detailed record of data from public organizations evidenced this [14]. The data obtained from SINCA (National Air Quality Information Service) [15] were chosen according to communes of the Metropolitan Region that have a more complete time series. The number of communes of the Metropolitan Region for which the SINCA carries out hourly measurements of meteorology and pollutants is 14, and 7 were eliminated. The databases with missing data (the amount of missing data in 2 communes (Las Condes, La Florida) was less than 2%) were completed using Nearest Neighbor filling techniques [16–20]. The pollutants considered, which have important effects on the respiratory tract of people among many other effects on human health, produced a picture of the existing diseases prior to the arrival of the pandemic in the country.

The Metropolitan Region has connected urban meteorology due to thermal islands (Figure 1) and urban canyons, apart from the basin geography that the area itself possesses. Many local climatic zones are present depending on the size and complexity of the Metropolitan Region. Thus, sectors can be recognized according to their predominant socio-economical features. These sectors form socially constructed climates based on the purchasing power of their inhabitants (which affects planning, urban management, the quality of construction, etc.) and can be highly connected to their interior, which favors the

spread of a disease [13]. A change in roughness is generated by high-rise construction and high urban densification, and then, together with urban micrometeorology and pollutants, a new thermal balance (thermal island) is created that makes the pandemic spread more effectively [4].

Cumulative Sick Data

Figure 3 presents the accumulated number of sick patients by communes in this study according to the period from 31 March 2020 to 9 January 2023.

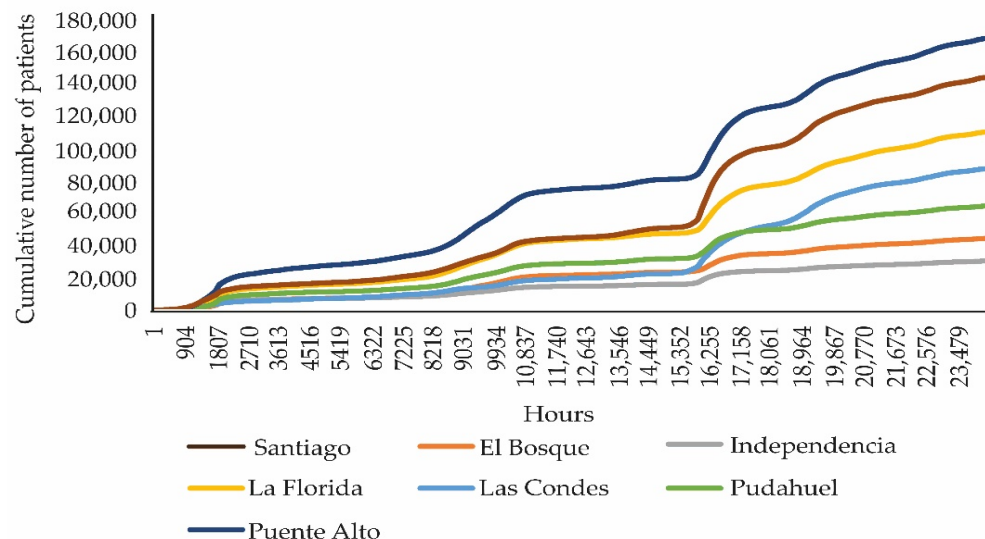


Figure 3. The accumulated diseases that occurred every hour in the seven communes of Santiago de Chile according to the study period [4].

The Metropolitan Region of Santiago de Chile currently (2023) accounts for 42% of the country's population. Table 2 shows the population according to the last census in 2017, patients accumulated by the pandemic, per capita income, and the multidimensional poverty index in the seven communes studied. Chaos theory was used to calculate the Kolmogorov entropy of the time series that relates accumulated sickness, meteorological variables (or urban meteorology), and pollutants. This relationship can be used to analyze the probabilities of heavy tails that influence the sustainability of the pandemic [21]. The accumulated sick (AS) records, obtained from the Ministry of Health of Chile (MINSAL), are summarized in Table 2 along with the communes considered in this study and their inhabitants [4,22].

Table 2. The communes considered in this study with their inhabitants.

Commune (2017)	Population (2017)	Accumulated Sick (31 March 2020–9 January 2023)	People per Capita Income in USD	Multidimensional Poverty Index [22]
Santiago	404,496	141,401	471	5–10%
Independencia	100,281	29,960	127	20–25%
Las Condes	294,838	85,890	1317	<5%
Puente Alto	568,106	165,038	175	20–25%
El Bosque	162,505	43,638	188	20–25%
La Florida	366,916	108,264	209	15–20%
Pudahuel	230,293	63,290	335	20–25%
Total	2,127,435	637,481	2822	

Table 3 shows, in an approximate way, the rate of growth of the square meters built and the number of patients accumulated in some of the communes of this study, showing that in the commune of Puente Alto (PA), there is a high level of overcrowding.

Table 3. Approximate variation in square meters built in five communes of this study [23–25] and the accumulated sick patients (31 March 2020–9 January 2023) [4]. The sixth column shows that the three communes with the highest density of inhabitants have the greatest number of accumulated patients.

Commune	2010 m ²	2020 m ²	Δm ²	AS (31 March 2020–09 January 2023)	Inhabitant Density hab/km ² [22]
La Florida	44,054	118,300	74,246	108,264	5227
Las Condes	127,342	145,306	17,964	85,890	2977
Santiago	94,043	190,862	96,819	141,401	17,436
Pudahuel	18,788	63,090	44,302	63,290	1000
Puente Alto	226,665	292,000	65,335	165,038	6456

2.3. Mathematical Tools

2.3.1. Chaos Theory

The hypothesis that non-linear processes were involved in the expansion of the pandemic supports the application of chaos theory to the constructed time series. Therefore, it is necessary to know some concepts of this theory.

A chaotic system is explained by a strange attractor that forms irregular orbits in a phase space. A strange attractor manifests itself when two adjacent points diverge exponentially. Furthermore, chaos depends on the initial conditions (butterfly effect). The Lyapunov exponent (λ) quantitatively describes this phenomenon. If a high dependence on initial conditions is detected in a system, it can be considered chaotic. Finding the Lyapunov exponent (λ_L) with the highest value in a time series is a sign that the system is chaotic. If $\lambda > 0$, then there is divergence between neighboring trajectories. When considering a one-dimensional dynamic system $x_{n+1} = f(x_n)$, λ is defined [22–24] as follows:

$$\lambda = \lim_{n \rightarrow \infty} \ln \left(\prod_{i=1}^{n-1} \left| \frac{df(x)}{dx} \right|_{x=x_i} \right) = \lambda = \lim_{n \rightarrow \infty} \ln \left(\prod_{i=0}^{n-1} \ln \left| \frac{df(x)}{dx} \right|_{x=x_i} \right) \quad (1)$$

The determination of λ can be carried out according to two procedures. The first procedure [26] is used for time series with time dependence and noise-free and small vectors in a neighboring space with highly non-linear evolution. The second method, called Jacobian, is applied for time series with large noise and linear evolution. This study applies the first case, where λ_L was calculated considering the length n of the single-variable time series X_1, X_2, \dots, X_n , given the phase points $Y_i = (x_i, x_{i-1}, \dots, x_{i+(m-1)})$ (where m is the embedding dimension). To examine the divergence in the exponential function, for the close orbits of chaotic motion [26], all phase points $N = n - (m - 1)\tau$ (with τ delay time) were selected as the reference point, where the reference phase point Y_i and the nearest phase space neighbor reference phase point Y_{ir} are the starting point of the nearby orbits. For time i , the orbital distance is the initial distance (Euclidean distance):

$$\delta_0^i = \|Y_i - Y_{ir}\| = \frac{1}{m} \sqrt{\sum_{k=1}^m (x_{i-(k-1)\tau} - x_{ir-(k-1)\tau})^2} \quad (2)$$

The exponential divergence between nearby trajectories of the chaotic system is:

$$\delta_t = \delta_0 e^{\lambda t} \quad (3)$$

where δ_0 is the starting point and δ_t is the point at time t .

The largest Lyapunov exponent λ_L is:

$$\lambda_L = \frac{\ln \frac{\delta_t}{\delta_0}}{t} = \frac{\ln \delta_t}{t} - \frac{\ln \delta_0}{t} \quad (4)$$

For a given time series, the sum of all the positive Lyapunov exponents defines its Kolmogorov entropy (S_K) and its reciprocal defines the average predictability time, $T_P = 1/S_K$ [26–29]. Considering that the number of phase points is equal to N and that the neighboring points undergo evolution according to t , the average of the total distance away is:

$$\bar{\delta}_t = \frac{1}{N} \sum_{i=1}^N \delta_t^i \quad (5)$$

When graphing the curve $\ln \bar{\delta}_t$ against t , a straight line is drawn on the linear part of the curve, which gives the slope λ_L . To ensure stability in the calculation of Lyapunov exponents, it is necessary to have over 5000 data points [26,30].

The correlation dimension (D_C) is a very important quantity that describes the geometric characteristics of the strange attractor. The numerical value of D_C may be a reflection of the inherent complexity of atmospheric systems, etc. D_C allows for determining m for the reconstruction of the phase space of the time series by reporting whether the time series is generated by a dynamic process and the number of dynamic variables that can explain the atmospheric system. A widely used algorithm [31] is based on the determination of the correlation integral (if the number of points $N \rightarrow \infty$). The discrete formulation is based on a statistical method that focuses on the number of points within all circles of radius r normalized to 1, with an r large enough to include all points without counting any point twice. When considering a reconstructed phase space, it is necessary to find the distance between two phase points to quantify the maximum difference between the two vectors as follows:

$$|Y_i - Y_j| = \max_{1 \leq k \leq m} |x_{i-(k-1)\tau} - x_{j-(k-1)\tau}| = |Y_{ij}| = \sqrt{\sum_{k=0}^{m-1} (x_{i-(k-1)\tau} - x_{j-(k-1)\tau})^2} \quad (6)$$

The correlation sum considers all related phase points and the percentage of phase points of all possible N ($N - 1$)/2:

$$C(r) = \text{correlation sum} = \frac{2}{N(N-1)} \sum_{i=1}^N \sum_{j=i+1}^N \text{Heav}(r - |Y_i - Y_j|) \rightarrow C(m, r) \quad (7)$$

where $\text{Heav}(x)$ is the unitary Heaviside function:

$$\text{Heav}(x) = \begin{cases} 0, & x \leq 1 \\ 1, & x > 1 \end{cases} \quad (8)$$

The definition of the Correlation Dimension [27] is:

$$D_C = \text{Correlation Dimension} = \lim_{r \rightarrow 0} \frac{\ln C(r)}{\ln r} \quad (9)$$

If we have a lot of data and r tends to very small values, $C(r)$ can behave according to the power relationship:

$$C(r) \sim r^{D_C} \quad (10)$$

When plotting the coordinate system $\ln C(r)$ against $\ln r$, the slope of the linear part is D_C . The correlation entropy, K_2 [4,27], is defined as:

$$K_2 = \lim_{m \rightarrow \infty} \lim_{r \rightarrow 0} \lim_{N \rightarrow \infty} \log \frac{C(m, r)}{C(m + 1, r)} \quad (11)$$

where r is the radius of the circle or sphere. K_2 is zero, positive, or infinite for regular, chaotic, or random data, respectively.

Thus, it can be stated [4,27] that the correlation entropy, K_2 , is a lower bound of Kolmogorov's entropy, S_K . That is,

$$K_2 \sim S_K \quad (12)$$

Chaotic analysis [4,27,32,33] includes the iterated function system (IFS) fragmentation test. Symbolic dynamics allow for calculating the Lempel–Ziv complexity ($LZ > 0$) related to white noise. The numerical calculation is performed with software [33] that is applied to each time series (called X, Y, Z, U, W, and V) without missing data.

Information loss can be calculated according to:

$$\langle \Delta I \rangle = \langle I_{\text{NEW}} - I_{\text{OLD}} \rangle \geq \frac{-\lambda(i_0(t))}{\log 2} \quad (13)$$

The Lyapunov exponent, $\lambda_0 = \lambda(x_0) = \lambda(i_0(t))$ (in [bits/h]), represents the exponential separation between two trajectories, which were initially close, after N steps or iterations and contains a quantity of information, I, related to that separation $I(x_0)$. Two types of $\langle \Delta I \rangle$ were calculated as follows: one for the contribution of each P (pollutants: PM₁₀, PM_{2.5}, and O₃) to the accumulated sick and another for the contribution of each MV (meteorological variables: T, WS, and RH) to the accumulated sick.

2.3.2. Anomalous Diffusion

Physical and biological systems have been discovered in which the mean square displacement of the diffusing substance grows with time in the form of $\langle r^2(t) \rangle \propto t^\alpha$, where the value of the exponent divides the process' diffusive in two different regimes as follows: super-diffusion, for $\alpha > 1$, and sub-diffusion, for $\alpha < 1$, which are particular cases of so-called anomalous diffusion, as shown in Figure 4.

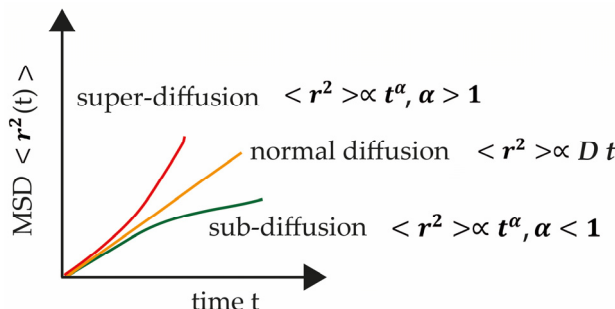


Figure 4. Mean square displacement of anomalous and normal diffusion.

The study and applications of anomalous diffusion, as an extended phenomenon, and like normal diffusion, escape the physical sciences. For the description and modeling of various complex systems, anomalous diffusion has been useful in the study of the internal structure of living cells, the characterization of the way in which different species of animals find food, etc.

The variance in quadratic displacement is:

$$\langle r^2 \rangle \propto t^\alpha \sim t^{\frac{S_{K,AS/MV}}{S_{K,AS/P}}} = t^{C_K} \quad (14)$$

The quadratic diffusive variance associated with the displacement in the AS/urban meteorology variables from the atmosphere to the interior of the boundary layer, close to the ground, is dependent on the interaction between the entropies of the AS/urban meteorology and the entropies of the AS/pollutants according to the C_K quotient.

The Fréchet distribution is a special case of an extreme value distribution or heavy-tailed distribution. The distribution function that represents it is:

$$\Pr(X \leq x) = e^{-x^{-\beta}} \text{ si } x > 0, \beta \in (0, \infty) \quad (15)$$

where $\beta > 0$ is the shape parameter. The generalization includes a location parameter, n , and a scale parameter, $s > 0$, resulting in:

$$\Pr(X \leq x) = e^{-(\frac{x-n}{s})^{-\beta}} \text{ si } x > n \quad (16)$$

In heavy-tailed distributions, there is a higher probability of extreme events compared with more commonly observed distributions such as the Gaussian or normal distributions. One of the fundamental concepts in heavy-tailed distributions is power law behavior, which occurs with the mean value of the squared variance in the position. Power law distributions present a scaling relationship between the probability density function and the variable of interest.

Table 4 shows the calculation of the maximum values, minimum values, standard deviation, average, and median for each of the time series of 24,360 accumulated patient data points, temperature, relative humidity, magnitude of wind speed, PM₁₀, PM_{2.5}, and O₃.

Table 4. Statistics of the time series of accumulated patients, meteorological variables, and pollutants of each commune (31 March 2020–9 January 2023).

	Pudahuel	Independencia	Santiago	Las Condes	La Florida	Pte. Alto	El Bosque
Accum. sick							
Deviation	19,575.06	8798.44	45,046.67	27,671.65	33,137.88	50,748.94	13,660.27
Average	30,047.79	15,354.37	57,472.85	30,443.55	47,098.76	76,376.38	21,138.38
Median	28,463.00	14,611.00	43,992.00	19,391.00	42,991.00	73,636.00	21,357.00
Temp (°C)							
Deviation	7.11	6.83	6.93	6.92	7.28	6.72	7.33
Average	14.51	15.17	15.26	13.99	15.33	14.68	13.61
Median	13.55	14.29	14.33	12.95	14.55	13.90	12.76
RH (%)							
Deviation	22.45	21.48	21.91	21.10	21.27	20.83	21.55
Average	63.89	61.18	63.20	59.44	58.85	58.92	59.09
Median	66.08	62.00	65.00	61.09	59.42	59.50	60.58
WS (m/s)							
Deviation	0.98	0.77	0.83	0.55	0.58	1.03	0.87
Average	1.13	0.94	0.91	0.82	0.78	1.27	0.98
Median	0.83	0.68	0.64	0.76	0.62	0.93	0.67
PM ₁₀ (µg/m ³)							
Deviation	46.53	39.86	38.15	29.50	40.52	36.30	48.00
Average	64.10	64.55	65.96	52.54	61.64	66.98	72.99
Median	51	55	57	47	53	61	61
PM _{2.5} (µg/m ³)							
Deviation	26.81	21.83	18.63	13.13	18.85	15.97	25.44
Average	26.00	24.39	22.97	17.44	23.68	22.22	28.93
Median	17	16	17	14	18	18	21
O ₃ (ppb)							
Deviation	15.12	16.60	17.24	19.27	18.34	16.75	14.86
Average	14.80	15.56	16.02	19.03	16.81	17.16	13.72
Median	10	9	10	12	10	12	8

Applying chaos theory [27,33] to the time series, the calculation of parameters $\lambda > 0$, $D_C < 5$, $S_K > 0$, $0.5 < H < 1$, $LZ > 0$ results in values that are in the required ranges. Therefore, the process is chaotic, and the results are summarized in Table 5.

Table 5. The results of the calculation of parameters including the Lyapunov coefficient (λ), correlation dimension (D_C), Kolmogorov entropy (S_K), Hurst exponent (H), Lempel–Ziv complexity (LZ), maximum time of predictability (T), and loss of information ($\langle \Delta I \rangle$) (31 March 2020, to 9 January 2023, 1,023,120 data points).

Comune	λ (bits/h)	D_c	S_K (bits/h)	H	LZ	$T = 1/S_K$ (h)	$\langle \Delta I \rangle$
Las Condes (LC)							
X	0.238 ± 0.015	2.099 ± 0.135	0.611	0.902570	0.10850	1.636	-0.791
Y	0.325 ± 0.026	3.098 ± 0.899	0.296	0.754360	0.09634	3.378	-1.079
Z	0.168 ± 0.013	3.852 ± 0.200	0.437	0.876525	0.47844	2.288	-0.558
			$S_{K, MV} = 1.344$	0.844485	0.22776	$\bar{T} = 2.434$	-2.428
W	0.179 ± 0.015	3.916 ± 0.238	0.477	0.871804	0.60284	2.096	-0.595
U	0.327 ± 0.021	4.369 ± 0.152	0.368	0.851004	0.61219	2.717	-1.086
V	0.499 ± 0.024	4.314 ± 0.133	0.398	0.871258	0.65148	2.513	-1.657
			$S_{K, P} = 1.243$	0.864688	0.62217	$\bar{T} = 2.442$	-3.338
Santiago (SANT)							
X	0.170 ± 0.013	4.024 ± 0.339	0.385	0.904362	0.36666	2.597	-0.565
Y	0.231 ± 0.020	1.575 ± 0.465	0.266	0.755542	0.08091	3.759	-0.767
Z	0.177 ± 0.013	4.078 ± 0.327	0.403	0.878623	0.51258	2.481	-0.588
			$S_{K, MV} = 1.054$	0.846175	0.32005	$\bar{T} = 2.946$	-1.920
W	0.248 ± 0.016	4.001 ± 0.277	0.447	0.876730	0.55280	2.096	-0.824
U	0.375 ± 0.022	3.672 ± 0.345	0.278	0.844136	0.48218	3.597	-1.246
V	0.336 ± 0.024	3.278 ± 0.156	0.106	0.936006	0.52988	9.434	-1.116
			$S_{K, P} = 0.831$	0.885624	0.52162	$\bar{T} = 5.042$	-3.186
Independencia (IND)							
X	0.222 ± 0.015	2.093 ± 0.148	0.543	0.902606	0.10710	1.842	-0.737
Y	0.353 ± 0.022	2.581 ± 0.881	0.308	0.812761	0.07249	3.246	-1.173
Z	0.133 ± 0.012	3.927 ± 0.235	0.436	0.891302	0.49808	2.294	-0.442
			$S_{K, MV} = 1.287$	0.868889	0.22589	$\bar{T} = 2.461$	-2.352
W	0.209 ± 0.014	3.755 ± 0.236	0.498	0.886482	0.60237	2.008	-0.694
U	0.307 ± 0.018	4.252 ± 0.154	0.506	0.884166	0.58367	1.976	-1.019
V	0.585 ± 0.025	3.824 ± 0.211	0.365	0.898487	0.60845	2.739	-1.943
			$S_{K, P} = 1.369$	0.889712	0.59816	$\bar{T} = 2.241$	-3.656
La Florida (LF)							
X	0.166 ± 0.012	4.116 ± 0.286	0.364	0.910665	0.35123	2.747	-0.551
Y	0.214 ± 0.020	1.374 ± 0.789	0.293	0.771460	0.08278	3.413	-0.711
Z	0.208 ± 0.014	4.449 ± 0.344	0.473	0.883141	0.50182	2.114	-0.691
			$S_{K, MV} = 1.130$	0.855088	0.31194	$\bar{T} = 2.758$	-1.953
W	0.295 ± 0.016	4.055 ± 0.300	0.448	0.873495	0.56215	2.232	-0.980
U	0.375 ± 0.022	4.073 ± 0.275	0.341	0.850949	0.50510	2.933	-1.246
V	0.792 ± 0.029	3.694 ± 0.405	0.357	0.916451	0.57852	2.655	-2.631
			$S_{K, P} = 1.146$	0.880298	0.54859	$\bar{T} = 2.760$	-4.857
Puente Alto (PA)							
X	0.130 ± 0.012	3.120 ± 0.234	0.419	0.905320	0.38537	2.386	-0.432
Y	0.607 ± 0.025	1.403 ± 0.572	0.293	0.793516	0.08605	3.413	-2.016
Z	0.181 ± 0.013	3.852 ± 0.228	0.374	0.891406	0.43354	2.674	-0.601
			$S_{K, MV} = 1.086$	0.863414	0.30165	$\bar{T} = 2.824$	-3.049
W	0.276 ± 0.016	4.406 ± 0.320	0.501	0.878464	0.50977	1.996	-0.917
U	0.415 ± 0.024	2.446 ± 0.650	0.072	0.868495	0.37882	13.888	-1.378
V	0.327 ± 0.024	2.403 ± 0.347	0.306	0.852885	0.54906	3.268	-1.086
			$S_{K, P} = 0.879$	0.866615	0.47922	$\bar{T} = 6.384$	-3.359
El Bosque (EB)							
X	0.231 ± 0.015	2.713 ± 0.111	0.608	0.908657	0.10616	1.645	-0.767
Y	0.424 ± 0.024	2.764 ± 0.906	0.355	0.820853	0.07717	2.817	-1.408
Z	0.192 ± 0.014	3.941 ± 0.249	0.437	0.887640	0.48171	2.288	-0.638
			$S_{K, MV} = 1.400$	0.872383	0.22168	$\bar{T} = 2.250$	-2.813
W	0.251 ± 0.016	3.601 ± 0.128	0.520	0.883469	0.61687	1.923	-0.833
U	0.319 ± 0.018	4.338 ± 0.178	0.537	0.872094	0.59068	1.862	-1.060
V	0.722 ± 0.028	4.360 ± 0.166	0.432	0.921180	0.60050	2.315	-2.398
			$S_{K, P} = 1.489$	0.892248	0.60268	$\bar{T} = 2.033$	-4.291
Pudahuel (P)							
X	0.242 ± 0.015	3.021 ± 0.181	0.242	0.908026	0.38256	4.132	-0.804
Y	0.143 ± 0.017	1.876 ± 0.571	0.230	0.737256	0.08325	4.347	-0.475
Z	0.174 ± 0.013	4.204 ± 0.372	0.398	0.891302	0.49808	2.513	-0.578
			$S_{K, MV} = 0.870$	0.845528	0.32130	$\bar{T} = 3.664$	-1.857
W	0.280 ± 0.016	3.967 ± 0.271	0.459	0.885674	0.56262	2.179	-0.930
U	0.386 ± 0.021	3.746 ± 0.189	0.346	0.860764	0.55841	2.890	-1.282
V	0.731 ± 0.028	3.795 ± 0.138	0.367	0.912855	0.58086	2.725	-2.428
			$S_{K, P} = 1.172$	0.886431	0.56730	$\bar{T} = 2.598$	-4.640

3. Results

The previous tables were summarized by extracting data that allowed for the construction of the figures. Thus, Table 6 shows the accumulated sick in each commune and the entropies of the ratios between (accumulated sick)/(pollutants) (or $S_{KAS,P}$) and (accumulated sick)/(meteorological variables) (or $S_{K,AS/MV}$). It also shows the calculated ratio between columns three and four, which was used to obtain C_K , whose formal definition is given below.

Table 6. The ratio between the entropies of (accumulated sick)/(meteorological variables) and the entropies of (accumulated sick)/(pollutants) and the accumulated sick (31 March 2020 to 9 January 2023).

Commune	AS	$S_{K, AS/MV}$	$S_{KAS,P}$	$C_K = S_{K, AS/MV}/S_{K, AS/P}$
La Florida (EML)	108,264	1.130	1.146	0.986
Las Condes (EMM)	85,890	1.344	1.243	1.081
Santiago (EMN)	141,401	1.054	0.831	1.268
Pudahuel (EMO)	63,290	0.870	1.172	0.742
Puente Alto (EMS)	165,038	1.086	0.879	1.235
El Bosque (EMQ)	43,638	1.400	1.489	0.940
Independencia (EMF)	29,960	1.287	1.369	0.940

From Table 6, it can be deduced that in four of the seven communes, the entropy of the ratio of (accumulated sick)/(pollutants) predominates, and in three of the seven communes, the entropy associated with the series of (accumulated sick)/(meteorological variables) dominates. From the perspective of the data and the entropic analysis, in the order of 20%, the ratio of (accumulated sick)/(pollutants) is higher than the ratio of (accumulated sick)/(meteorological variables), but both give sustainability to the pandemic. One of the communes triggered by the effect of urban weather is Puente Alto (EMS), which has a very high population density [4].

Figure 4 below shows, for the study period including confinement, the entropies of the ratio between (accumulated sick)/(meteorological variables) (temperature, relative humidity, magnitude of wind speed) and the entropies of the ratio between (accumulated sick)/(pollutants) (PM_{10} , $PM_{2.5}$, O_3) by commune together with the C_K ratio, which is defined as

$$C_{K, \text{communes}} = \frac{\sum \text{Entropy}_{(\text{Accumulated Sick})/(\text{Meteorological Variables})_{\text{communes}}}}{\sum \text{Entropy}_{(\text{Accumulated Sick})/(\text{Pollutants})_{\text{communes}}}} \quad (17)$$

When Figure 5 is analyzed for the entropy associated with the time series that relates accumulated patients and urban meteorology, it is found that the entropy of the meteorological variables is lower, with a more uniform behavior that is predictable and stable. The effect of pollutants on accumulated patients is reduced because there are fewer pollutants because of the lockdown. The pollutants are more chaotic and have greater entropy (this is concluded from the measurements), which affects the relationship with the accumulated patients. This is directly indicated in Figure 5, which shows that practically four of the seven communes are in the condition described.

Even so, the fastest loss of information, characteristic of a chaotic system, corresponds to the ratio of (accumulated sick)/(meteorological variables). As shown in Figure 6, which was obtained from the data in Table 5, the information losses per commune (eighth column) are added into the following two groups: (1) AS/T, AS/WS, AS/RH and (2) AS/ PM_{10} , AS/ $PM_{2.5}$, AS/ O_3 , and are graphed with the accumulated sick for each commune.

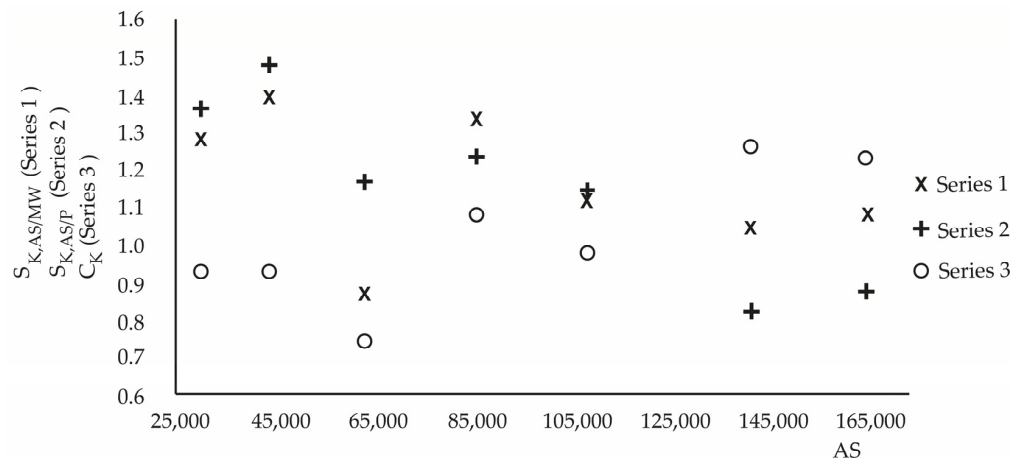


Figure 5. Comparison of the entropies of the ratio of (accumulated sick)/(meteorological variables) (Series 1), the ratio of (accumulated sick)/(pollutants) (Series 2), and the ratio between both entropies (Series 3) according to the accumulated sick by commune.

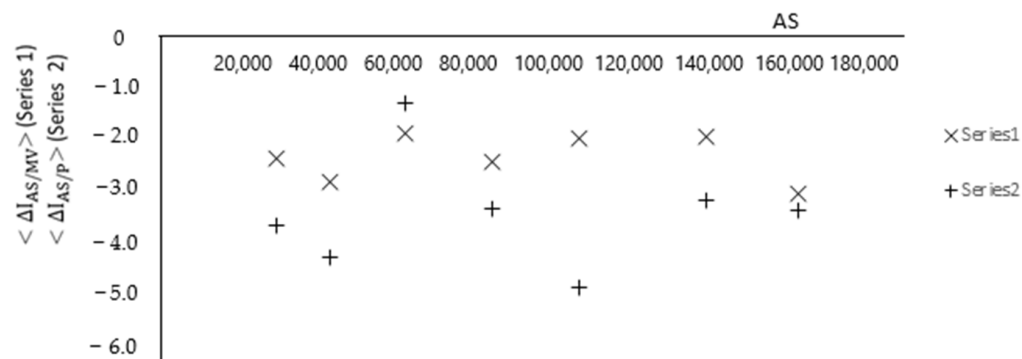


Figure 6. Series 1 corresponds to the loss of information in the ratio of (accumulated sick)/(meteorological variables), and Series 2 corresponds to the loss of information in the ratio of (accumulated sick)/(pollutants).

It can be seen from Table 6 that the diffusive effect of C_K is quite heterogeneous in the basin morphology, manifesting a super-diffusive effect with $\alpha > 1$, for the increase in accumulated sick patients. This is observed in at least three of the communes that have a large population, high urban densification, and high-rise buildings, another commune that almost falls at the limit between sub-diffusive and super-diffusive processes (La Florida) with $\alpha \sim 1$, and three communes with sub-diffusive regimes ($\alpha < 1$). The case of Pudahuel is quite exceptional because it is a commune that is subject to a mountain passageway effect that transports coastal influence. According to the second and fifth columns of Table 6, Figure 7 is obtained.

Table 7 specifies, according to locality, the probability by applying Fréchet distribution.

The Fréchet distribution tends to evolve in a similar way to the evolution towards super-diffusive regimes of the C_K parameter, that is, high urban and population densification and high-rise buildings that favor the spread of the virus, as shown in Figure 8.

Figure 5 shows that despite the reduction in human activity, air pollution is more persistent and more predictable than urban meteorology in most communes. From the perspective of urban meteorology, according to the values of the Hurst coefficients, which indicate the ability to influence the future, temperature, in particular, gives the greatest persistence to the ratio of (accumulated sick)/(temperature) compared with all the other meteorological variables and practically in all communes. Even so, the pollutant system is the most persistent compared with the urban micrometeorology system. The same is true for Lempel–Ziv complexity. The confinement favored an environmental improvement in the city of Santiago de Chile, according to Table 8.

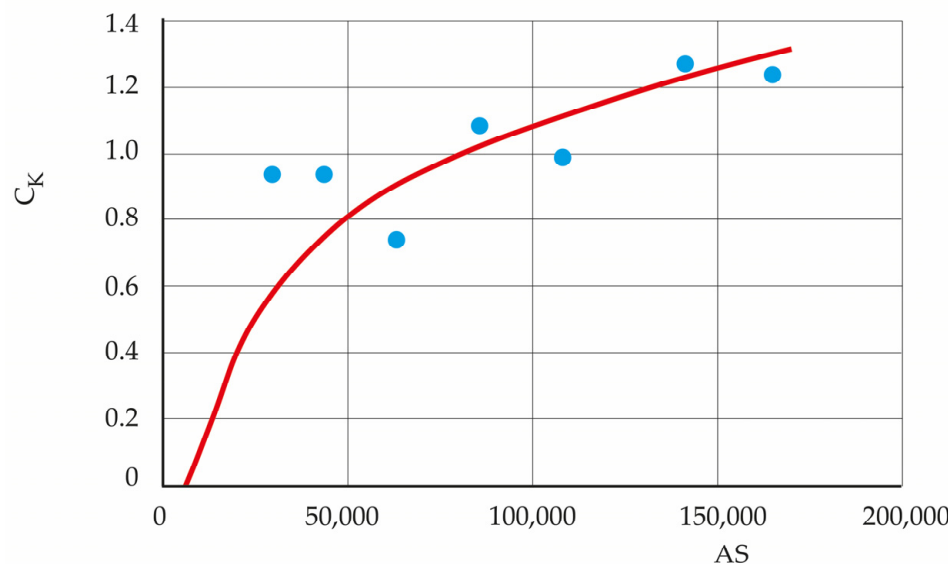


Figure 7. The evolution of C_K towards high population and urban and high-rise construction density.

Table 7. Location, number of accumulated sick patients in the study period, C_K , Fréchet probability distribution, and type of diffusion.

Localization	AS (31 March 2020–9 January 2023)	C_K (2020–2023)	Pr	Diffusion Type
EMO	63,290	0.74	0.28	sub diffusion
EMQ	43,638	0.94	0.35	sub diffusion
EMF	29,960	0.94	0.35	sub diffusion
EML	108,264	0.99	0.37	diffusion
EMM	85,890	1.08	0.39	super-diffusion
EMS	165,038	1.24	0.43	super-diffusion
EMN	141,401	1.27	0.44	super-diffusion

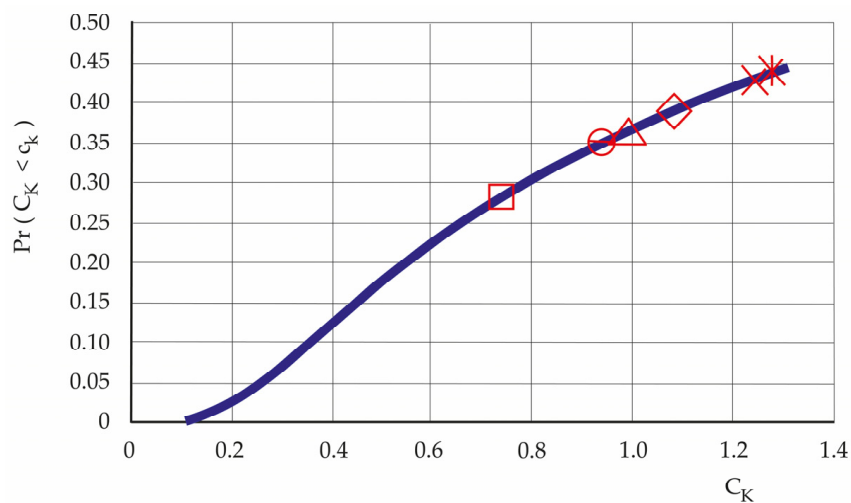


Figure 8. Fréchet probability distribution (with $\beta = 0.8$, $C_K \in (0, \infty)$) versus C_K . The probability of a heavy tail becomes greater as extreme events increase, which, in this case, is the accumulated patients (AS) \times : 165,038, \diamond : 85,890, Δ : 108,264, $-$: 29,960, o : 43,638, \square : 63,290.

Table 8. The average values of temperature and relative humidity according to three different periods.

	EML	EMM	EMV	EMN	EMS	EMO	Average by Commune
2010–2013							
\bar{T} (°C)	15.4	15.86	15.80	15.34	14.70	16.80	15.65
RH (%)	58.20	58.13	57.34	60.22	60.07	57.52	58.58
2017–2020							
\bar{T} (°C)	16.12	15.57	16.85	16.17	15.53	16.78	16.17
RH (%)	55.31	55.00	58.95	57.31	56.07	59.22	56.98
2019–2022							
\bar{T} (°C)	16.10	14.70	15.50	16.05	15.42	15.31	15.51
RH (%)	56.20	57.83	61.20	60.84	56.96	61.32	59.10

Table 8 indicates that in the period 2019–2022, the average temperature experienced a decrease and the average relative humidity increased when compared with the periods 2010–2013 and 2017–2020. This strengthening of urban meteorology makes it emerge as an element that favors, according to 42.86%, the growth in the entropy of (accumulated sick)/(meteorological variables). This marks a great difference compared with the studies of shorter periods [3 (2.5 months (30 March–15 June 2022)), 4 (25 months (30 March 2020–18 April 2022))], where the polluting system, exclusively, increased the entropy of the ratio of (accumulated sick)/(pollutants) compared with that of the ratio of (accumulated sick)/(meteorological variables). Here, in the study of the extended period, from 31 March 2020 to 9 January 2023, in three of the seven communes, urban meteorology increased the entropy of the ratio of (accumulated sick)/(meteorological variables). This is also a demonstration of the versatility and adaptability of the pandemic, which can use all means, such as urban weather, which is very difficult to control, as an element that cooperates in maintaining or increasing the sustainability of the virus. This is combined in a good way with the times of maximum predictability of the ratio of (accumulated sick)/(meteorological variables) and of the ratio of (accumulated sick)/(pollutants) where, in four (EMM, EMF, EML, EMQ) of the seven communes, the value is very similar. This shows the greater influence that urban meteorology acquires, in periods of decreased human activity, on the ratio of (accumulated sick)/(pollutants) and marks a difference compared with the studies [3,4]. The period of confinement covered practically 2 years (2020–2021).

Table 9 provides a summary of the perspective of the actions undertaken by the political and health authorities.

Table 9. The actors in the city's work that are oriented actions that affect various human activities. This can be verified according to various instances and the effects it had on the life of the city (hard confinement: period March 2020–March 2022).

Actors	Human Activities	Check	Effects
population	mandatory use of a mask, confinement of the population to their homes, vaccination process of the population (two and three doses), increase in hospital beds and equipment, orders for essential goods delivered to homes, attention in commerce (supermarkets, etc.) by small groups of people, street signs to maintain distances among people	Ministry of Health, police from Chilean Companies	deserted streets, irruption of wildlife in the city, crime reduction
culture and information	improvement in personal hygiene, development of a culture of hygiene in public and private facilities, permanent information on the pandemic through the media, companies, educational establishments, etc.	Ministry of Health, Ministry of Education, Media	learning
travels	mobility passes for people with full doses of vaccines, reduced travel by air, land, and sea except for very justified cases, police and military control of routes, mobility passes requested at police stations	SINCA, measurements, police from Chile	entropy calculation, control of the population

Table 9. Cont.

Actors	Human Activities	Check	Effects
teaching and work	teaching via the internet, work via the internet, financial aid vouchers for workers, pension fund withdrawals, boxes with food and toiletries	educational centers closed, companies with no or very little activity, Congress, SINCA	low quality of learning, disorders psychological, overweight
wildlife	lockdown of the population in their homes	Media, population, wildlife organizations	irruption of wild fauna in cities

4. Discussion

This study complements [3,4] by considering data extended to almost a year after the end of the confinement. The results demonstrate, based on Table 6, Figure 5, and Table 9, the effect of the pandemic on human activity. As an important sidenote, wild animals enjoyed the freedom of a calmer world when the global coronavirus lockdown gave parts of the natural world a rare opportunity to experience life with hardly any humans around [34,35].

Based on the analysis of the data from a geographic basin, it can be deduced that temperature makes the ratio between (accumulated sick)/(temperature) more persistent, and relative humidity makes it more complex, considering the effect of the meteorological variables measured in the extended period (31 March 2020 to January 9, 2023; 1,023,120 data points) of the coronavirus 2 (SARS-CoV-2) pandemic, and that can cause severe acute respiratory syndrome [36,37]. Although Baker [37] used a climate-dependent epidemic model to simulate the SARS-CoV-2 pandemic, testing different climate-dependence scenarios based on known coronavirus biology, susceptibility levels among the population remain the determining factor that drives the pandemic. Without the application of effective controls, the pandemic will persist in the coming months, causing severe outbreaks even in humid climates (Santiago de Chile is dry, aggravated by a drought of nearly 30 years). The summer will not substantially limit the growth of the pandemic, which is something that this investigation confirms. The most significant difference compared to [37] is that this study is based on measurements recorded at ground level (a height between 2 and 10 m), which is where ordinary citizens live and is very complex to incorporate into a simulation.

Until now, the most notable result has been that for confinement, according to the data record of the extended period, the effect of urban meteorology and that of pollution reduced by confinement on the accumulated patients are distributed with very similar probabilities. This goes back to the argument of achieving immunity for the entire population. This does not mean that the climate is not important in the long term.

The analysis procedure does not identify the details of the effect of each season of the year, so it can only be added that it is probable that the endemic cycles of the disease are linked to climatic factors. The technique is very specific in determining which urban meteorology variable helps to make the curve of accumulated sick patients more sustainable and, in turn, makes it possible to compare the effect of the urban meteorological system and the polluting system on the accumulated sick. Urban meteorology begins to show the effect of stopping pollution due to confinement.

Thus, this research provides a qualitative description based on quantitative variables—such as temperature, relative humidity, and the magnitude of the wind speed—which are basic descriptions of climatic factors, the effect of the confinement regime on them, and their incidence in the sustainability of a pandemic. This allows for understanding the implications of control measures on the duration of immunity. It also shows that it is not enough to consider urban meteorology in the study of the pandemic and that air pollution plays a role. Both participate in its sustainability [4] (see Table 6 and Figure 5 above), which is the connected way in which all entropic processes in nature work [36,38].

In [39], it was concluded that the lockdown in England was the only measure that consistently reduced R, the average number of people a person with COVID-19 will infect,

to below 1. And the sooner the measures were applied, the better. Another study [40] reached similar conclusions.

Wu [41] and colleagues examined three different response strategies for SARS-CoV-19 in eight countries and argued that aggressive containment is the optimal approach to limit the loss of life and livelihoods, which can be achieved in the absence of effective vaccines and therapies as follows: aggressive containment (in 28 days); suppression by implementing public health interventions (protecting vulnerable (lockdowns, masks, etc.) and high-risk groups while allowing transmission among low-risk groups); and mitigation trying to avoid overloading health systems by flattening the epidemic curve or achieving herd immunity in the population.

Non-pharmaceutical interventions [42], such as social distancing and lockdowns, have been essential to control the coronavirus disease 2019 (COVID-19) pandemic. Localized lockdowns in small geographic areas have become an important policy intervention to prevent viral spread in cases of resurgence. These localized lockdowns can have lower social and economic costs relative to larger-scale suppression strategies. Using an integrated data set from Chile (3 March to 15 June 2020, an exceptionally short study period) and an original synthetic control treatment, the effect of localized blockages was estimated, clarifying their direct and indirect causal effects on coronavirus 2 (SARS-CoV-2) transmission. Although the results indicated that the effects of localized lockdowns were strongly modulated by their duration and influenced by the indirect effects of neighboring geographical areas, leaving out urban densification, micrometeorology, and air pollution, which is the environment of people's lives, conditioned the results.

In [43], daily data of confirmed cases of COVID-19 (172,746) from the Casablanca region together with meteorological parameters (average temperature, wind, relative humidity, precipitation, duration of sunshine) and air quality (CO , NO_2 , O_3 , SO_2 , PM_{10}) for the period from 2 March 2020 to 31 December 2020 were analyzed with the General Additive Model (GAM). Positive associations were determined between COVID-19 and wind ($>20 \text{ m/s}$) and relative humidity ($>80\%$). For temperatures $>25^\circ\text{C}$, there was a negative association with daily cases of COVID-19. PM_{10} and O_3 had a positive effect on increasing the number of daily confirmed cases of COVID-19, while precipitation had a limiting effect below 25 mm and a negative effect above this value.

Ref. [44] also linked exposure to $\text{PM}_{2.5}$ and coarse PM_{10} with adverse outcomes of COVID-19, including increased incidence and mortality. Applying a less biased method such as Mendelian randomization (MR), which uses genetic variants as instrumental variables to infer causal relationships in observational data, it was possible to establish a causal relationship between pollution by smaller particles, specifically $\text{PM}_{2.5}$, and a greater risk of severity and hospitalization due to COVID-19.

In this study, an approach based on measurements of accumulated patients, urban meteorology, and pollutants, the pandemic phenomenon that affected different communes of Santiago de Chile is described. The initial conditions of the places studied consider the unexpected appearance of a highly contagious virus, urban densification, urban meteorology, atmospheric pollution, high-rise buildings, overcrowding, accumulated sick patients, etc. This interdisciplinary topic is addressed with procedures that include chaos theory, anomalous diffusion, and Fréchet heavy-tailed probability [45]. The difference compared with other more theoretical investigations [46–48] is in the robustness of the measured data (amount of data over a million) and the good agreement presented by the three methods used.

5. Conclusions

A total of 1,023,120 data points were processed with measurements deep inside the boundary layer at the ground level, which were distributed in 42 time series, showing that all were chaotic with characteristic parameters including the Lyapunov exponent (λ), the correlation dimension (D_C), Kolmogorov entropy (S_K), the Hurst exponent (H), Lempel-Ziv complexity (LZ), and loss of information ($\langle \Delta I \rangle$) in the appropriate ranges. The analysis of these parameters made it possible to demonstrate that the confinement reduced air

pollution, improving, in part, urban meteorology. Unlike shorter measurement periods (2.5 and 25 months), where confinement did not show its effect on pollution, this study, conducted over an extended period (34.25 months), shows that its influence becomes effective on urban meteorology. Healthy urban weather does not guarantee a stop in the spread of the pandemic. What it indicates is that rather both systems, polluting + urban meteorology, jointly contribute to the sustainability of the accumulated sick patients due to the pandemic. The percentages show that in four of the seven communes, the entropy of the ratio between the accumulated sick and pollutant is dominant, even with confinement. However, in three of the seven communes, the time series of the ratio between the accumulated sick and urban meteorology prevails. This indicates that confinement plus vaccination of the entire population give more guarantees of immunity and that they are important factors to apply to the dynamics of pandemic invasion, which can use the conditions of urban densification, the urban climate, and the pollution that is generated for its expansion. The scenarios posed by the pandemic are very complex and connected, covering, among many other aspects, urban micrometeorology, air pollution, urban densification, the geographical distribution of confinements, the vulnerable population, etc. Chaos theory, anomalous diffusion, and Fréchet's heavy-tailed probability distribution achieve similar and consistent results for the topic.t

Author Contributions: Conceptualization, P.P.; methodology, P.P.; software, P.P. and G.N.; validation, P.P., E.M. and G.N.; formal analysis, P.P.; investigation, P.P. and E.M.; resources, E.M.; data curation, E.M.; writing—original draft preparation, P.P.; writing—review and editing, P.P. and E.M.; visualization, P.P. and E.M.; supervision, P.P.; project administration, P.P.; funding acquisition, P.P. All authors have read and agreed to the published version of the manuscript.

Funding: This research was supported by ANID/CONICYT/FONDECYT Regular 1240127. This publication had the support of the Vicerrectoría de Investigación y Doctorados de la Universidad San Sebastián – Fondo USS-FIN-24-APCS-07.

Institutional Review Board Statement: Not applicable.

Informed Consent Statement: Informed consent was obtained from all subjects involved in this study.

Data Availability Statement: The data were obtained from the public network for online monitoring of air pollutant concentration and meteorological variables. The network is distributed throughout all of Chile, without access restrictions. It is the responsibility of SINCA, the National Air Quality Information System, dependent on the Environment Ministry of Chile. The data for the two study periods are available for free use on the WEB page: URL: <https://sinca.mma.gob.cl>, accessed on 11 January 2023.

Acknowledgments: To the Research Directorate of the Universidad Tecnológica Metropolitana (UTEM) that made possible the progress of this study and to the Department of Physics of the UTEM for their collaboration.

Conflicts of Interest: The authors declare no conflicts of interest.

References

1. Pacheco, P.; Mera, E.; Fuentes, V. Intensive Urbanization, Urban Meteorology and Air Pollutants: Effects on the Temperature of a City in a Basin Geography. *Int. J. Environ. Res. Public Health* **2023**, *20*, 3941. [[CrossRef](#)] [[PubMed](#)]
2. Pacheco, P.; Mera, E. Relations between Urban Entropies, Geographical Configurations, Habitability and Sustainability. *Atmosphere* **2022**, *13*, 1639. [[CrossRef](#)]
3. Salini, G.A.; Pacheco, P.R.; Mera, E.; Parodi, M.C. Probable relationship between COVID-19, pollutants and meteorology: A case study at Santiago, Chile. *Aerosol Air Qual. Res.* **2021**, *21*, 200434. [[CrossRef](#)]
4. Pacheco, P.; Mera, E. Study of the Effect of Urban Densification and Micrometeorology on the Sustainability of a Coronavirus-Type Pandemic. *Atmosphere* **2022**, *13*, 1073. [[CrossRef](#)]
5. Neeltje van Doremalen, N.; Bushmaker, T.; Morris, D.H.; Holbrook, M.G.; Gamble, A.; Williamson, B.N.; Tamin, A.; Harcourt, J.L.; Thornburg, N.J.; Gerber, S.I.; et al. Aerosol and Surface Stability of SARS-CoV-2, as Compared with SARS-CoV-1. *N. Engl. J. Med.* **2020**, *382*, 1564–1567. [[CrossRef](#)]
6. Gramsch, E.; Morales, L.; Baeza, M.; Ayala, C.; Soto, C.; Neira, J.; Pérez, P.; Moreno, F. Citizens' Surveillance Micro-network for the Mapping of PM2.5 in the City of Concón, Chile. *Aerosol Air Qual. Res.* **2020**, *20*, 358–368. [[CrossRef](#)]

7. Đorđević, D.; Milanković, J.D.; Pantelić, A.; Petrović, S.; Gambaro, A. Coarse, fine and ultrafine particles of suburban-continental aerosols measured using an 11-stage Berner cascade impactor. *Atmos. Pollut. Res.* **2020**, *11*, 499–510. [[CrossRef](#)]
8. Iwasaka, Y.; Minoura, H.; Nagaya, K. The transport and spacial scale of Asian dust-storm clouds: A case study of the dust-storm event of April 1979. *Tellus B Chem. Phys. Meteorol.* **1983**, *35*, 189–196. [[CrossRef](#)]
9. WHO/Europe. *Review of Evidence on Health Aspects of Air Pollution—REVIHAAP Project Technical Report*; World Health Organization, Regional Office for Europe: Copenhagen, Denmark, 2013. Available online: <https://www.eea.europa.eu/data-and-maps-indicators/exceedance-of-air-quality-limit-3/who-2013> (accessed on 27 November 2022).
10. Nuvolone, D.; Petri, D.; Voller, F. The effects of ozone on human health. *Environ. Sci. Pollut. Res.* **2018**, *25*, 8074–8088. [[CrossRef](#)]
11. Díaz, J.; Ortiz, C.; Falcón, I.; Salvador, C.; Linares, C. Short-term effect of tropospheric ozone on daily mortality in Spain. *Atmos. Environ.* **2018**, *187*, 107–116. [[CrossRef](#)]
12. Byass, P. Eco-epidemiological assessment of the COVID-19 epidemic in China, January–February 2020. *Glob. Health Action* **2020**, *13*, 1760490. [[CrossRef](#)] [[PubMed](#)]
13. Iqbal, N.; Fareed, Z.; Shahzad, F.; He, X.; Shahzad, U.; Lina, M. The nexus between COVID19, temperature and exchange rate in Wuhan city: New findings from partial and multiple wavelet coherence. *Sci. Total Environ.* **2020**, *729*, 138916. [[CrossRef](#)] [[PubMed](#)]
14. MINSAL (Chilean Ministry of Health). Available online: <https://www.minsal.cl/> (accessed on 15 January 2023).
15. SINCA (Chilean Air Quality National Information System). Available online: <https://sinca.mma.gob.cl> (accessed on 30 January 2023).
16. Silverman, B.W.; Jones, M.C.; Fix, E. An Important Contribution to Nonparametric Discriminant Analysis and Density Estimation: Commentary on Fix and Hodges (1951). *Int. Stat. Rev.* **1989**, *57*, 233–238. [[CrossRef](#)]
17. Junninen, H.; Niska, H.; Tuppurainen, K.; Ruuskanen, J.; Kolehmainen, M. Methods for imputation of missing values in air quality data sets. *Atmos. Environ.* **2004**, *38*, 2895–2907. [[CrossRef](#)]
18. Norazian, M.N.; Shruki, Y.A.; Azam, R.M.; Mustafa Al Bakri, A.M. Estimation of missing values in air pollution data using single imputation techniques. *ScienceAsia* **2008**, *34*, 341–345. [[CrossRef](#)]
19. Emery, X. Simple and ordinary multigaussian Kriging for estimating recoverable reserves. *Math. Geol.* **2005**, *37*, 295–319. [[CrossRef](#)]
20. Asa, E.; Saafi, M.; Membah, J.; Billa, A. Comparison of linear and nonlinear Kriging methods for characterization and interpolation of soil data. *J. Comput. Civil Eng.* **2012**, *26*, 11–18. [[CrossRef](#)]
21. Pacheco, P.; Mera, E.; Salini, G. Medición Localizada de Contaminantes Atmosféricos y Variables Meteorológicas: Segunda Ley de la Termodinámica. *Inf. Tecnol.* **2019**, *30*, 105–116. [[CrossRef](#)]
22. Census. XIX Censo Nacional de Población y VIII de Vivienda o Censo de Población y Vivienda 2017, Gobierno de Chile e Instituto Nacional de Estadísticas de Chile. 2017. Available online: <https://www.ine.cl> (accessed on 23 November 2022).
23. INE-Plataforma de Datos Estadísticos. Available online: https://www.ine.es/ine/planine/informe_anual_2019.pdf (accessed on 11 December 2022).
24. MVU, Ministerio de Vivienda y Urbanismo (Ministry of Housing and Urbanism); Centro de Estudios de Ciudad y Territorio. Available online: <https://www.observatoriourbano.cl> (accessed on 3 January 2023).
25. Government of Chile. Official Data COVID-19. Available online: <https://www.gob.cl/coronavirus/cifrasoficiales/> (accessed on 18 January 2023).
26. Salini, G.; Pérez, P. A study of the dynamic behavior of fine particulate matter in Santiago, Chile. *Aerosol Air Qual. Res.* **2015**, *15*, 154–165. [[CrossRef](#)]
27. Sprott, J.C. *Chaos and Time-Series Analysis*, 1st ed.; Oxford University Press: Oxford, UK, 2003.
28. Manríquez, R. Estructuras disipativas. De la termodinámica a la psicoterapia familiar. *Rev. Asoc. Española Neuropsiquiatría* **1987**, *VII*, 435–454.
29. Chen, Y.; Wang, J.; Feng, J. Understanding the Fractal Dimensions of Urban Forms through spatial. *Entropy* **2017**, *19*, 600. [[CrossRef](#)]
30. Wolf, A.; Swift, J.B.; Swinney, H.L.; Vastano, J.A. Determining Lyapunov exponents from a time series. *Phys. D* **1985**, *16*, 285–317. [[CrossRef](#)]
31. Grassberger, P.; Procaccia, L. Characterization of Strange Attractors. *Phys. Rev. Lett.* **1983**, *50*, 346–349. [[CrossRef](#)]
32. Horna Mercedes, J.; Dionicio Vereau, J.; Martínez Zocón, R.; Zavaleta Quipuscoa, A.; Brenis Delgado, Y. Dinámica simbólica y algunas aplicaciones. *Sel. Matemáticas* **2016**, *3*, 101–106. [[CrossRef](#)]
33. Sprott, J.C. Chaos Data Analyzer Software. 1995. Available online: <http://sprott.physics.wisc.edu/cda.htm> (accessed on 4 April 2023).
34. Green, D.G. Connectivity and the evolution of biological systems. *J. Biol. Syst.* **1994**, *2*, 91–103. [[CrossRef](#)]
35. Zellmer, A.J.; Wood, E.M.; Surasinghe, T.; Putman, B.J.; Pauly, G.B.; Magle, S.B.; Lewis, J.S.; Kay, C.A.M.; Fidino, M. What can we learn from wildlife sightings during the COVID-19 global shutdown? *Ecosphere* **2020**, *11*, e03215. [[CrossRef](#)]
36. Sahin, O.; Salim, H.; Suprun, E.; Richards, R.; MacAskill, S.; Heilgeist, S.; Rutherford, S.; Stewart, R.A.; Beal, C.D. Developing a Preliminary Causal Loop Diagram for Understanding the Wicked Complexity of the COVID-19 Pandemic. *Systems* **2020**, *8*, 20. [[CrossRef](#)]
37. Baker, R.E.; Yang, W.; Vecchi, G.A.; Metcalf, C.J.E.; Grenfell, B.T. Susceptible supply limits the role of climate in the COVID-19 pandemic. *Science* **2020**, *369*, 315–319. [[CrossRef](#)]

38. Pacheco Hernández, P.R.; Salini Calderón, G.A.; Mera Garrido, E.M. Entropía y Neguentropía: Una aproximación al proceso de difusión de contaminantes y su sostenibilidad. *Rev. Int. Contam. Ambient.* **2021**, *37*, 167–185. [[CrossRef](#)]
39. Lewis, D. What scientists have learnt from COVID lockdowns. *Nature* **2022**, *609*, 236–239. [[CrossRef](#)] [[PubMed](#)]
40. Chen, S.; Guo, L.; Alghaith, T.; Dong, D.; Alluhidan, M.; Hamza, M.M.; Herbst, C.H.; Zhang, X.; Tagtag, G.C.A.; Zhang, Y.; et al. Effective COVID-19 Control: A Comparative Analysis of the Stringency and Timeliness of Government Responses in Asia. *Int. J. Environ. Res. Public Health* **2021**, *18*, 8686. [[CrossRef](#)]
41. Wu, S.; Neill, R.; De Foo, C.; Chua, A.Q.; Jung, A.S.; Haldane, V.; Abdalla, S.M.; Guan, W.J.; Singh, S.; Nordström, A.; et al. Aggressive containment, suppression, and mitigation of COVID-19: Lessons learnt from eight countries. *BMJ* **2021**, *375*, e067508. [[CrossRef](#)]
42. Li, Y.; Undurraga, E.A.; Zubizarreta, J.R. Effectiveness of Localized Lockdowns in the COVID-19 Pandemic. *Am. J. Epidemiol.* **2022**, *191*, 812–824. [[CrossRef](#)] [[PubMed](#)]
43. Khalis, M.; Toure, A.B.; El Badisy, I.; Khomsi, K.; Najmi, H.; Bouaddi, O.; Marfak, A.; Al-Delaimy, W.K.; Berraho, M.; Nejjari, C. Relationship between Meteorological and Air Quality Parameters and COVID-19 in Casablanca Region, Morocco. *Int. J. Environ. Res. Public Health* **2022**, *19*, 4989. [[CrossRef](#)] [[PubMed](#)]
44. Zhu, J.; Zhou, Y.; Lin, Q.; Wu, K.; Ma, Y.; Liu, C.; Liu, N.; Tu, T.; Liu, Q. Causal relationship between particulate matter and COVID-19 risk: A mendelian randomization study. *Heliyon* **2024**, *24*, e27083. [[CrossRef](#)] [[PubMed](#)]
45. Fontanelli, O.; Mansilla, R.; Miramontes, P. Probability distributions in the complexity sciences: A contemporary perspective. *Inter. Discip.* **2020**, *8*, 11–37. [[CrossRef](#)]
46. Shah, K.; Sinan, M.; Abdeljawad, T.; El-Shorbagy, M.A.; Abdalla, B.; Abualrub, M.S. A Detailed Study of a Fractal-Fractional Transmission Dynamical Model of Viral Infectious Disease with Vaccination. *Complexity* **2022**, *2022*, 7236824. [[CrossRef](#)]
47. Sinan, M.; Alharthi, N.H. Mathematical Analysis of Fractal-Fractional Mathematical Model of COVID-19. *Fractal Fract.* **2023**, *7*, 358. [[CrossRef](#)]
48. El-Borai, M.; El-Nadi, K. Stochastic Fractional Models of the Diffusion of COVID-19. *Adv. Math. Sci. J.* **2020**, *9*, 10281–10293. [[CrossRef](#)]

Disclaimer/Publisher’s Note: The statements, opinions and data contained in all publications are solely those of the individual author(s) and contributor(s) and not of MDPI and/or the editor(s). MDPI and/or the editor(s) disclaim responsibility for any injury to people or property resulting from any ideas, methods, instructions or products referred to in the content.